



# Highly selective synthesis of *para*-diethylbenzene by alkylation of ethylbenzene with diethyl carbonate over boron oxide modified HZSM-5



Bing Xue<sup>a</sup>, Gen Zhang<sup>a</sup>, Na Liu<sup>a</sup>, Jie Xu<sup>a</sup>, Qingming Shen<sup>b</sup>, Yongxin Li<sup>a,\*</sup>

<sup>a</sup> Jiangsu Key Laboratory of Advanced Catalytic Materials and Technology, School of Petrochemical Engineering, Changzhou University, Changzhou 213164, China

<sup>b</sup> Institute of Advanced Materials, Nanjing University of Posts and Telecommunications, Nanjing 210046, China

## ARTICLE INFO

### Article history:

Received 29 May 2014

Received in revised form 28 August 2014

Accepted 28 August 2014

Available online 6 September 2014

### Keywords:

Shape-selective catalysis

*para*-Diethylbenzene

B<sub>2</sub>O<sub>3</sub>/HZSM-5

Triethyl borate

## ABSTRACT

A series of B<sub>2</sub>O<sub>3</sub>/HZSM-5 catalysts were prepared by impregnation of HZSM-5 zeolites with triethyl borate, trimethyl borate and boric acid. The selective synthesis of *para*-diethylbenzene by alkylation of ethylbenzene with diethyl carbonate was carried out over the B<sub>2</sub>O<sub>3</sub>/HZSM-5 catalysts. The physico-chemical properties of the catalysts were characterized by X-ray diffraction, N<sub>2</sub> adsorption–desorption, Fourier-transform infrared spectroscopy with pyridine adsorption and NH<sub>3</sub> temperature programmed desorption. The characterization results indicated that the 15% B<sub>2</sub>O<sub>3</sub>/HZSM-5 catalyst prepared by using triethyl borate as the precursor exhibited an outstanding shape-selectivity along with a high catalytic activity in alkylation of ethylbenzene with diethyl carbonate. This might be ascribed to the large molecular size of triethyl borate, which would lead to the formation of B<sub>2</sub>O<sub>3</sub> on the external surface of HZSM-5 zeolite and preserve the acid sites in the micropores of HZSM-5 zeolite. By contrast, the B<sub>2</sub>O<sub>3</sub>/HZSM-5 catalysts prepared by using trimethyl borate or boric acid led to the severe reduction in catalytic activity, which was attributed to the decrease in the amount of the total acid sites caused by the blockage of the partial pores of HZSM-5 zeolite.

© 2014 Elsevier B.V. All rights reserved.

## 1. Introduction

*Para*-diethylbenzene (*p*-DEB) is a high-valued aromatic. It is extensively used as a desorbent in the adsorptive separation process of *para*-xylene, such as UOP Para-ex [1]. Besides, it is also a starting material for the synthesis of divinylstyrene [2]. Two processes, i.e. ethylbenzene (EB) alkylation [3,4] and EB disproportionation [5,6], have been developed for the production of *p*-DEB. HZSM-5 zeolite could be the best catalyst for the production *p*-DEB because of its unusual shape-selectivity [7]. However, the acid sites on the external surface of HZSM-5 zeolite caused some side reactions, such as the isomerization of *p*-DEB, which always decreased the *para*-selectivity. Therefore, it is necessary to passivate the acid sites on the external surface of zeolite to obtain the desired *para*-selectivity. Many approaches have been developed to modify the surface property of HZSM-5 to promote the *para*-selectivity, including SiO<sub>2</sub>-CVD [8–10], SiO<sub>2</sub>-CLD [11,12], pre-cooking [13,14] and impregnation of metal or non-metal compounds [15–19]. Although

SiO<sub>2</sub>-CVD or SiO<sub>2</sub>-CLD modification with simple silicon alkoxides could greatly improve the *para*-selectivity, these processes were complicated. Pre-cooking was often difficult to control, and needed to be repeated after the recovered zeolite catalysts were regenerated by calcination. By contrast, covering the external acid sites of zeolite with metal or non-metal compounds was a convenient method. Metal or non-metal oxides could be used to eliminate the external surface acid sites of zeolites, while this would also cover the acid sites in the channels and decrease the catalytic activity of zeolites. Therefore, a simple and efficient strategy for deactivating the acid sites on the external surface of zeolite without influencing the acid sites in the channels of zeolite was required.

We have developed a novel method for preparing MgO modified MCM-22 shape-selective catalysts using a complexation–impregnation method [20–24]. During the complexation impregnation process, when the molecular size of the complex is larger than the pore entrance of the MCM-22 zeolites, Mg<sup>2+</sup> can be confined to the external surface of the zeolite. This not only covered the external acid sites, but also prevented the deactivation of the acid sites in the channels of zeolite. Based on the creativity mentioned above, we tried to develop a new way to prepare shape-selective catalyst: using compounds with larger

\* Corresponding author. Tel.: +86 519 86330135; fax: +86 519 86330135.

E-mail address: liyxluck@163.com (Y. Li).

molecular size, such as triethyl borate, as the precursor of  $B_2O_3$  to prepare oxide modified zeolite shape-selective catalysts. Results confirmed that a high shape-selectivity along with a high catalytic activity was obtained in the production of *p*-DEB by alkyltaion of EB with diethyl carbonate (DEC) over the boron oxide modified HZSM-5 catalysts. This method is effective and innovative for the preparation of shape-selective catalysts developed to date. In the present study, boron oxide modified HZSM-5 shape-selective catalysts were prepared by selecting a series of borate with different molecular size and the catalytic performances of these catalysts for *para*-alkylation of EB with DEC were investigated in detail.

## 2. Experimental

### 2.1. Catalyst preparation

ZSM-5 zeolite ( $Si/Al=50$ ) was synthesized by hydrothermal crystallization according to an established procedure [25]. The  $NH_4^+$  form of the as synthesized ZSM-5 zeolites was obtained by ion-exchange with aqueous  $NH_4NO_3$  solution, and then calcined at 823 K for 3 h. The boron oxide modified HZSM-5 catalysts was prepared as follows. The borate, including trimethyl borate and triethyl borate, was dissolved in dehydrated alcohol. HZSM-5 was impregnated with an ethanol solution containing borate. The mixture was stirred for 1 h and allowed to stand overnight. Afterwards, the mixture was evaporated in a constant temperature bath at 353 K for 6 h and then dried in an oven at 383 K for 6 h. Then, the resulting materials were calcined at 823 K for 5 h in an air stream. The obtained catalyst was denoted as  $x\% B_2O_3/HZSM-5(M)$  or  $B_2O_3/HZSM-5(E)$ , where the  $x$  represented the mass percentage of  $B_2O_3$  based on the supports. The M and E represent the precursor of  $B_2O_3$  in the catalysts is from trimethyl borate or triethyl borate, respectively. In contrast, boric acid was also used as the precursor of  $B_2O_3$  to prepare  $B_2O_3/ZSM-5$  catalysts, and the catalysts were denoted as  $x\% B_2O_3/ZSM-5(H)$ .

### 2.2. Catalyst characterization

X-ray diffraction (XRD) measurements were conducted using a Rigaku D/max2500PC diffractometer with  $Cu K\alpha$  ( $\lambda = 1.54 \text{ \AA}$ ) radiation. The diffractograms were recorded in  $2\theta$  range 5–50° in steps of 0.02° with a count time of 15 s.

$N_2$  adsorption/desorption analyses were obtained at 77 K using a physical adsorption instrument (Micromeritics ASAP 2020, USA). Before measurement, the samples were degassed at 523 K under vacuum until a final pressure of  $1 \times 10^{-3} \text{ kPa}$  was reached. The specific surface area was calculated according to the Brunauer–Emmett–Teller (BET) isothermal equation.

Sample acidity was measured by  $NH_3$  temperature-programmed desorption ( $NH_3$ -TPD) using a Quantachrome CHEMBET-3000 instrument. A 200 mg sample was pre-treated at 823 K for 1 h in dry helium (flowing at  $50 \text{ mL min}^{-1}$ ), cooled to 393 K, then exposed to 10% v/v  $NH_3/He$  mixture for 0.5 h. After purging the catalyst with He for 0.5 h, the TPD plot was obtained at a heating rate of  $10 \text{ K min}^{-1}$  from 393 to 823 K. The thermal conductivity detector (TCD) signal and temperature corresponding to  $NH_3$  desorption were recorded simultaneously. The amount and temperature of the desorbed  $NH_3$  corresponded qualitatively to the amount and strength of the acid sites.

FT-IR spectra of the samples were recorded using a Bruker FT-IR spectrometer (TENSOR 27) with the KBr pellet technique. Spectra were recorded in the range  $4000$ – $400 \text{ cm}^{-1}$ .

FT-IR spectra with pyridine and 2,4-dimethylquinoline (2,4-DMQ) adsorption was carried out using a Bruker FT-IR spectrometer (TENSOR 27) together with a high temperature vacuum chamber.

The scanning range was from 1700 to  $1400 \text{ cm}^{-1}$  and the resolution was  $4 \text{ cm}^{-1}$ . The sample powder was pressed into a self-supporting wafer. Prior to each experiment, the catalysts were evacuated (1 Pa) at 653 K for 3 h, and then cooled at 303 K for 2 h, and then exposed to 4 kPa of pyridine or 2,4-DMQ solubilized in  $CH_2Cl_2$  (30  $\mu\text{mol}$  for 1 mL solvent) for 5 min, and finally evacuated for 1 h at 303 K. After adsorption of pyridine the samples were heated to 473 K at  $10 \text{ K min}^{-1}$  and the spectra were recorded.

Cracking of 1,3,5-triisopropylbenzene (1,3,5-TIPB) and cumene (IPB) was carried out using a fix bed reactor at 723 K under  $N_2$  flow with a WHSV (weight hourly space velocity) of  $1 \text{ h}^{-1}$ . The catalysts were tested for 1 h on stream. The products were analyzed by gas chromatography (GC-2010, SHIMADZU) using a FFAP capillary column and flame ionization detector (FID).

### 2.3. Alkylation of EB with DEC

Alkylation of EB with DEC was carried out in a fixed bed continuous down-flow reactor. About 3 g of the catalyst (as pellets of 20–40 mesh) was packed in the middle of the reactor and calcined in a dry nitrogen flow for about 1 h at 653 K before reaction. The reaction mixture of EB with DEC was introduced at the top of the reactor by means of an infusion pump. The products were collected in a water-cooled condenser attached to the end of the reactor and analyzed by gas chromatography (GC-2010, SHIMADZU) using a FFAP capillary column and flame ionization detector.

## 3. Results and discussion

### 3.1. Catalytic performances of $B_2O_3/ZSM-5$ catalysts

The catalytic performances of  $B_2O_3/ZSM-5(E)$ ,  $B_2O_3/ZSM-5(M)$  and  $B_2O_3/ZSM-5(H)$  catalysts in the synthesis of *p*-DEB by alkylation of EB with DEC were presented in Tables 1–3, respectively. As shown in Table 1, HZSM-5 exhibited the highest conversion of EB among the investigated catalysts. However, the selectivity for *p*-DEB over HZSM-5 was poor. After modification with triethyl borate, the conversion of EB over  $B_2O_3/ZSM-5(E)$  catalysts decreased gradually from 48.2% to 31.3% with increasing the amount of  $B_2O_3$  to 18%. Notably, a relatively high conversion of EB was retained even for 18%  $B_2O_3/ZSM-5(E)$  catalyst. Meanwhile, the selectivity for *p*-DEB over  $B_2O_3/ZSM-5(E)$  catalysts increased obviously with increasing the amount of  $B_2O_3$ . The highest selectivity for *p*-DEB, about 97.6%, was observed over 18%  $B_2O_3/ZSM-5(E)$  catalyst. The catalytic performances of  $B_2O_3/ZSM-5(M)$  and  $B_2O_3/ZSM-5(H)$  catalysts in alkylation of EB with DEC differed from those of  $B_2O_3/ZSM-5(E)$  catalysts. Although the selectivity for *p*-DEB over  $B_2O_3/ZSM-5(M)$  or  $B_2O_3/ZSM-5(H)$  catalysts was also significantly improved with increasing the amount of  $B_2O_3$ , the catalytic activities decreased severely, as shown in Tables 2 and 3. As for 15%  $B_2O_3/ZSM-5$  catalysts, the conversion of EB over  $B_2O_3/ZSM-5(E)$  catalyst was markedly higher than those over  $B_2O_3/ZSM-5(M)$  and  $B_2O_3/ZSM-5(H)$  catalysts. In particular, only a 2.3% conversion of EB was acquired over 15%  $B_2O_3/ZSM-5(H)$  catalyst.

### 3.2. Catalysts characterizations

Fig. 1 shows the XRD patterns of HZSM-5 and  $B_2O_3/HZSM-5(E)$  catalysts with different  $B_2O_3$  loadings. Compared with HZSM-5, no obvious changes in the position of peaks belonging to HZSM-5 zeolite were detected in the XRD patterns of the  $B_2O_3/HZSM-5(E)$  catalysts. This indicated that the structure of HZSM-5 zeolite was retained without any significant changes after modification with triethyl borate. The peaks due to  $B_2O_3$  were not observed even for 15%  $B_2O_3/HZSM-5(E)$  catalyst. The XRD patterns of 15%

**Table 1**Catalytic performance of  $\text{B}_2\text{O}_3/\text{HZSM-5(E)}$  catalysts in alkylation of EB with DEC.

Samples	Conversion of EB (%)	Products distribution of DEB (%)		
		<i>p</i> -DEB	<i>m</i> -DEB	<i>o</i> -DEB
HZSM-5	48.2	33.2	66.3	0.5
3% $\text{B}_2\text{O}_3/\text{HZSM-5(E)}$	40.7	38.7	60.1	1.2
6% $\text{B}_2\text{O}_3/\text{HZSM-5(E)}$	35.8	59.4	39.9	0.7
9% $\text{B}_2\text{O}_3/\text{HZSM-5(E)}$	33.1	80.1	19.6	0.3
12% $\text{B}_2\text{O}_3/\text{HZSM-5(E)}$	32.5	94.0	5.5	0.5
15% $\text{B}_2\text{O}_3/\text{HZSM-5(E)}$	31.0	97.0	2.8	0.2
18% $\text{B}_2\text{O}_3/\text{HZSM-5(E)}$	31.3	97.6	2.2	0.2

Reaction conditions:  $T = 633 \text{ K}$ , 6 h,  $n(\text{EB})/n(\text{DEC}) = 2:1$ , LHSV =  $1 \text{ h}^{-1}$ .**Table 2**Catalytic performance of  $\text{B}_2\text{O}_3/\text{HZSM-5(M)}$  catalysts in alkylation of EB with DEC.

Samples	Conversion of EB (%)	Products distribution of DEB (%)		
		<i>p</i> -DEB	<i>m</i> -DEB	<i>o</i> -DEB
3% $\text{B}_2\text{O}_3/\text{HZSM-5(M)}$	36.3	35.2	64.3	0.5
6% $\text{B}_2\text{O}_3/\text{HZSM-5(M)}$	32.9	39.7	60.1	0.2
9% $\text{B}_2\text{O}_3/\text{HZSM-5(M)}$	27.9	51.7	47.4	0.9
12% $\text{B}_2\text{O}_3/\text{HZSM-5(M)}$	20.1	78.9	19.6	1.5
15% $\text{B}_2\text{O}_3/\text{HZSM-5(M)}$	16.2	85.5	13.7	0.8

Reaction conditions:  $T = 633 \text{ K}$ , 6 h,  $n(\text{EB})/n(\text{DEC}) = 2:1$ , LHSV =  $1 \text{ h}^{-1}$ .**Table 3**Catalytic performance of  $\text{B}_2\text{O}_3/\text{ZSM-5(H)}$  catalysts in alkylation of EB with DEC.

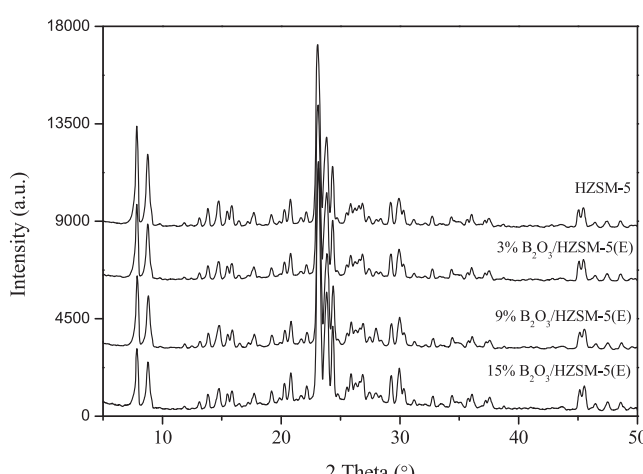
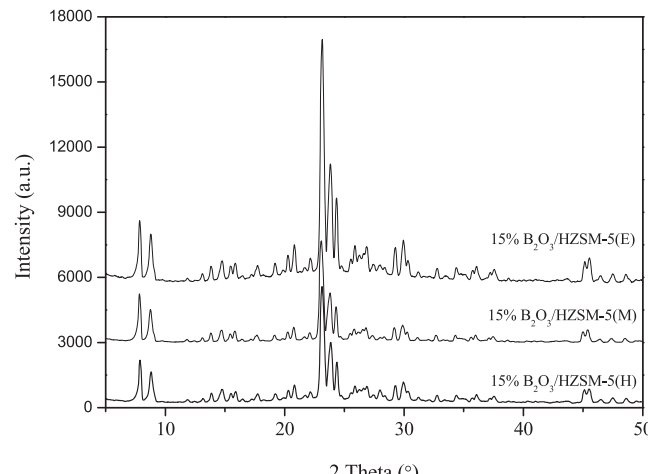
Samples	Conversion of EB (%)	Products distribution of DEB (%)		
		<i>p</i> -DEB	<i>m</i> -DEB	<i>o</i> -DEB
3% $\text{B}_2\text{O}_3/\text{ZSM-5(H)}$	34.1	34.2	63.1	2.7
6% $\text{B}_2\text{O}_3/\text{ZSM-5(H)}$	28.4	45.7	54.3	0.0
9% $\text{B}_2\text{O}_3/\text{ZSM-5(H)}$	12.4	68.1	30.4	1.5
12% $\text{B}_2\text{O}_3/\text{ZSM-5(H)}$	4.2	99.2	0.5	0.3
15% $\text{B}_2\text{O}_3/\text{ZSM-5(H)}$	2.1	99.1	0.5	0.4

Reaction conditions:  $T = 633 \text{ K}$ , 6 h,  $n(\text{EB})/n(\text{DEC}) = 2:1$ , LHSV =  $1 \text{ h}^{-1}$ .

$\text{B}_2\text{O}_3/\text{HZSM-5}$  catalysts with different precursor of  $\text{B}_2\text{O}_3$  were presented in Fig. 2. Similarly, no peaks corresponding to  $\text{B}_2\text{O}_3$  were detected over 15%  $\text{B}_2\text{O}_3/\text{HZSM-5(M)}$  and 15%  $\text{B}_2\text{O}_3/\text{HZSM-5(H)}$  catalysts. Careful examination of Fig. 2 revealed that the intensities of peaks belonging to HZSM-5 zeolite in the XRD patterns of 15%  $\text{B}_2\text{O}_3/\text{HZSM-5(H)}$  and 15%  $\text{B}_2\text{O}_3/\text{HZSM-5(M)}$  samples were obviously lower than that of 15%  $\text{B}_2\text{O}_3/\text{HZSM-5(E)}$  catalyst.

The FT-IR spectra of the 15%  $\text{B}_2\text{O}_3/\text{HZSM-5}$  catalysts with different precursor of  $\text{B}_2\text{O}_3$  were shown in Fig. 3. The asymmetric stretching, symmetric stretching and bending vibrations of

Si–O–Si were observed at 1100, 800 and  $450 \text{ cm}^{-1}$ , respectively. The absorptions at 1230 and  $550 \text{ cm}^{-1}$  corresponded to the presence of five-membered ring chains and different ring structures, respectively. These features were basically identical for the HZSM-5 zeolite [26,27]. This indicated that the structure of HZSM-5 zeolite was well preserved after  $\text{B}_2\text{O}_3$  modification. Compared with the FT-IR spectrum of HZSM-5, obvious absorptions at  $1409 \text{ cm}^{-1}$  were presented on the spectra of the 15%  $\text{B}_2\text{O}_3/\text{HZSM-5}$  catalysts, which was ascribed to the B–O stretching [28,29]. This

**Fig. 1.** XRD patterns of HZSM-5 and  $\text{B}_2\text{O}_3/\text{HZSM-5(E)}$  catalysts.**Fig. 2.** XRD patterns of 15%  $\text{B}_2\text{O}_3/\text{HZSM-5}$  catalysts with different precursor of  $\text{B}_2\text{O}_3$ .

**Table 4**

Textural parameters of the  $\text{B}_2\text{O}_3/\text{HZSM-5(E)}$  catalysts.

Samples	$A_{\text{BET}}$ ( $\text{m}^2 \text{g}^{-1}$ )	$A_{\text{M}}$ ( $\text{m}^2 \text{g}^{-1}$ )	$A_{\text{E}}$ ( $\text{m}^2 \text{g}^{-1}$ )	$V_{\text{T}}$ ( $\text{cm}^3 \text{g}^{-1}$ )	$V_{\text{M}}$ ( $\text{cm}^3 \text{g}^{-1}$ )	$V_{\text{Me}}$ ( $\text{cm}^3 \text{g}^{-1}$ )
HZSM-5	374	267	107	0.245	0.141	0.104
3% $\text{B}_2\text{O}_3/\text{HZSM-5(E)}$	317	258	59	0.181	0.139	0.042
9% $\text{B}_2\text{O}_3/\text{HZSM-5(E)}$	288	230	58	0.163	0.123	0.040
15% $\text{B}_2\text{O}_3/\text{HZSM-5(E)}$	259	213	46	0.167	0.117	0.050

$A_{\text{BET}}$ , BET surface area;  $A_{\text{M}}$ , micropore area;  $A_{\text{E}}$ , external surface area;  $V_{\text{T}}$ , total pore volume;  $V_{\text{M}}$ , micropore volume;  $V_{\text{Me}}$ , mesopore volume.

**Table 5**

Textural parameters of 15%  $\text{B}_2\text{O}_3/\text{HZSM-5}$  catalysts.

Sample	$A_{\text{BET}}$ ( $\text{m}^2 \text{g}^{-1}$ )	$A_{\text{M}}$ ( $\text{m}^2 \text{g}^{-1}$ )	$A_{\text{E}}$ ( $\text{m}^2 \text{g}^{-1}$ )	$V_{\text{T}}$ ( $\text{cm}^3 \text{g}^{-1}$ )	$V_{\text{M}}$ ( $\text{cm}^3 \text{g}^{-1}$ )
15% $\text{B}_2\text{O}_3/\text{HZSM-5(E)}$	259	213	46	0.167	0.117
15% $\text{B}_2\text{O}_3/\text{HZSM-5(M)}$	179	164	15	0.117	0.089
15% $\text{B}_2\text{O}_3/\text{HZSM-5(H)}$	123	110	13	0.085	0.058

$A_{\text{BET}}$ , BET surface area;  $A_{\text{M}}$ , micropore area;  $A_{\text{E}}$ , external surface area;  $V_{\text{T}}$ , total pore volume;  $V_{\text{M}}$ , micropore volume.

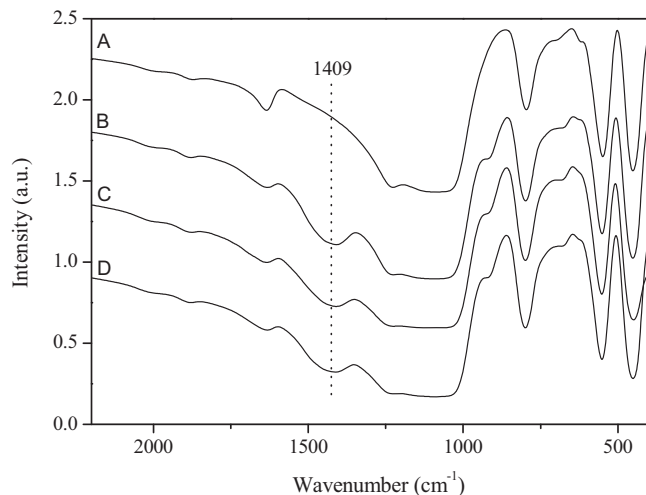


Fig. 3. FT-IR spectra of HZSM-5 and 15%  $\text{B}_2\text{O}_3/\text{HZSM-5}$  catalysts. (A) HZSM-5; (B) 15%  $\text{B}_2\text{O}_3/\text{HZSM-5(E)}$ ; (C) 15%  $\text{B}_2\text{O}_3/\text{HZSM-5(M)}$ ; (D) 15%  $\text{B}_2\text{O}_3/\text{HZSM-5(H)}$ .

confirmed the formation of  $\text{B}_2\text{O}_3$  over the surface of  $\text{B}_2\text{O}_3/\text{HZSM-5}$  zeolite.

The isotherms for HZSM-5 and  $\text{B}_2\text{O}_3/\text{HZSM-5}$  catalysts were displayed in Figs. 4 and 5. The textural parameters of the  $\text{B}_2\text{O}_3/\text{HZSM-5}$  catalysts were summarized in Tables 4 and 5. It can be seen that

all the isotherms of the samples are of type I, showing characteristics of micro-porous zeolite type materials: large increase of adsorbed  $\text{N}_2$  at low pressure range followed by nearly horizontal adsorption/desorption branches [30]. As for the isotherms of HZSM-5 zeolite, a small hysteresis loop appearing at  $p/p^0 > 0.95$ , most probably related to the interparticle voids of HZSM-5 zeolite, which mainly contributed to the external surface and the mesopore volume of the zeolite. After modification with  $\text{B}_2\text{O}_3$  by using triethyl borate as the precursor, the hysteresis loop appearing at  $p/p^0 > 0.95$  decreased significantly. This may be ascribed to the cover of the  $\text{B}_2\text{O}_3$  on the external surface area of HZSM-5 zeolite. As shown in Table 4, the BET surface area and the micropore volume of  $\text{B}_2\text{O}_3/\text{HZSM-5(E)}$  catalysts decreased gradually with increasing the amount of  $\text{B}_2\text{O}_3$ . It was worth noting that a high BET surface area (about  $259 \text{ m}^2 \text{ g}^{-1}$ ) was maintained even for 15%  $\text{B}_2\text{O}_3/\text{HZSM-5(E)}$  catalyst. The mesopore volume of HZSM-5 and  $\text{B}_2\text{O}_3/\text{HZSM-5(E)}$  catalysts were also presented in Table 4. After modification with  $\text{B}_2\text{O}_3$ , the mesopore volume of  $\text{B}_2\text{O}_3/\text{HZSM-5(E)}$  catalysts decreased obviously compared with HZSM-5 zeolite. However, no obvious difference in the mesopore volume of  $\text{B}_2\text{O}_3/\text{HZSM-5(M)}$  and 15%  $\text{B}_2\text{O}_3/\text{HZSM-5(H)}$  is obviously lower than those of 15%  $\text{B}_2\text{O}_3/\text{HZSM-5(E)}$ . Especially for 15%  $\text{B}_2\text{O}_3/\text{HZSM-5(H)}$  catalyst, only a BET surface area of  $123 \text{ m}^2 \text{ g}^{-1}$  and a micropore volume of  $0.058 \text{ cm}^3 \text{ g}^{-1}$  were observed.

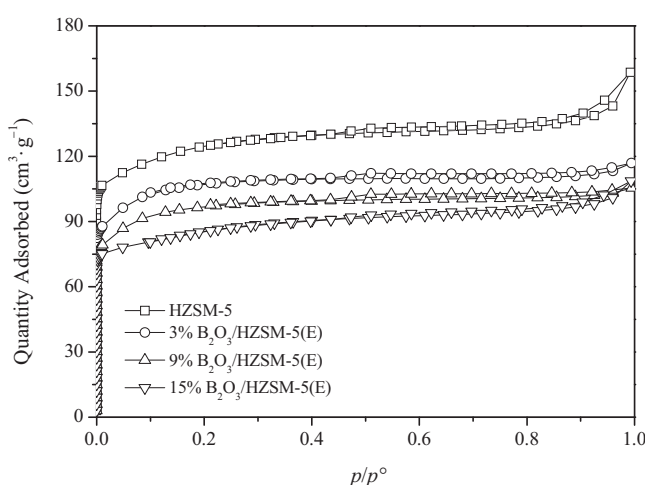


Fig. 4.  $\text{N}_2$  adsorption/desorption isotherms of HZSM-5 and  $\text{B}_2\text{O}_3/\text{HZSM-5(E)}$  catalysts.

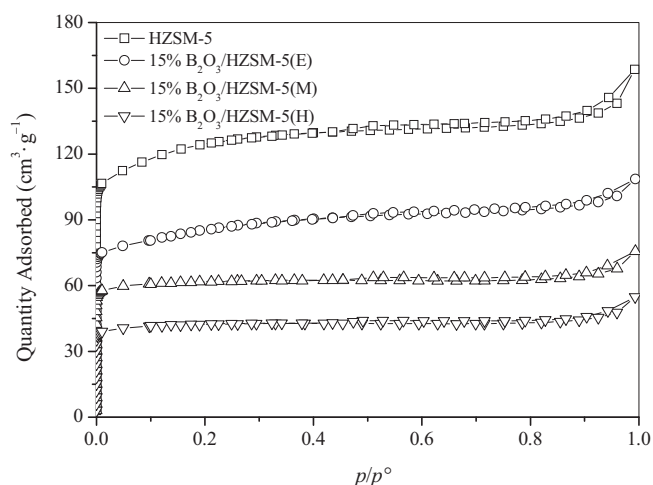
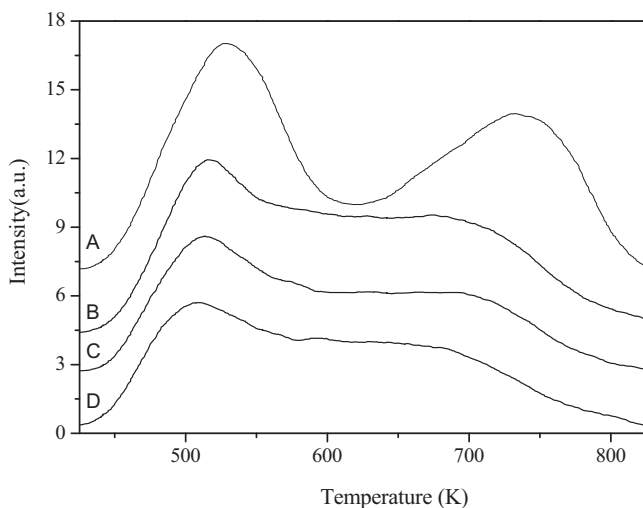


Fig. 5.  $\text{N}_2$  adsorption/desorption isotherms of HZSM-5 and 15%  $\text{B}_2\text{O}_3/\text{HZSM-5}$  catalysts with different precursor of  $\text{B}_2\text{O}_3$ .



**Fig. 6.**  $\text{NH}_3$ -TPD profiles of HZSM-5 and  $\text{B}_2\text{O}_3/\text{HZSM-5(E)}$  catalysts. (A) HZSM-5; (B) 3%  $\text{B}_2\text{O}_3/\text{HZSM-5(E)}$ ; (C) 9%  $\text{B}_2\text{O}_3/\text{HZSM-5(E)}$ ; (D) 15%  $\text{B}_2\text{O}_3/\text{HZSM-5(E)}$ .

The  $\text{NH}_3$ -TPD profiles of HZSM-5 and  $\text{B}_2\text{O}_3/\text{HZSM-5(E)}$  catalysts are presented in Fig. 6. It can be observed that all the samples exhibit the typical double-peak characteristic of zeolites with MFI structure [31]. As for HZSM-5 zeolite, the strong peak at about 520 K can be associated with the desorption of physisorbed ammonia and/or ammonia adsorbed on weak acid sites, and the strong peak at about 730 K may be attributed to the desorption of ammonia adsorbed on strong acid sites [32]. It was found that the areas of high temperature and low temperature peaks of  $\text{B}_2\text{O}_3/\text{HZSM-5(E)}$  catalysts decreased with an increase in the amount of  $\text{B}_2\text{O}_3$ , and the position of desorption temperature shifted slightly to lower temperature. These results indicate the modification with triethyl borate decreased the total amount of the acid sites, especially for the strong acid sites. Fig. 7 showed the  $\text{NH}_3$ -TPD profiles of 15%  $\text{B}_2\text{O}_3/\text{HZSM-5}$  catalysts with different precursor of  $\text{B}_2\text{O}_3$ . Obviously, the total amount of the acid sites of 15%  $\text{B}_2\text{O}_3/\text{HZSM-5(M)}$  and 15%  $\text{B}_2\text{O}_3/\text{HZSM-5(H)}$  is clearly lower than that of 15%  $\text{B}_2\text{O}_3/\text{HZSM-5(E)}$ . In particular, the strong acid sites over 15%  $\text{B}_2\text{O}_3/\text{HZSM-5(M)}$  and 15%  $\text{B}_2\text{O}_3/\text{HZSM-5(H)}$  catalysts had almost disappeared compared with 15%  $\text{B}_2\text{O}_3/\text{HZSM-5(E)}$  catalyst.

FT-IR spectra with pyridine adsorption of HZSM-5 and  $\text{B}_2\text{O}_3/\text{HZSM-5(E)}$  catalysts were illustrated in Figs. 8 and 9. Pyridine

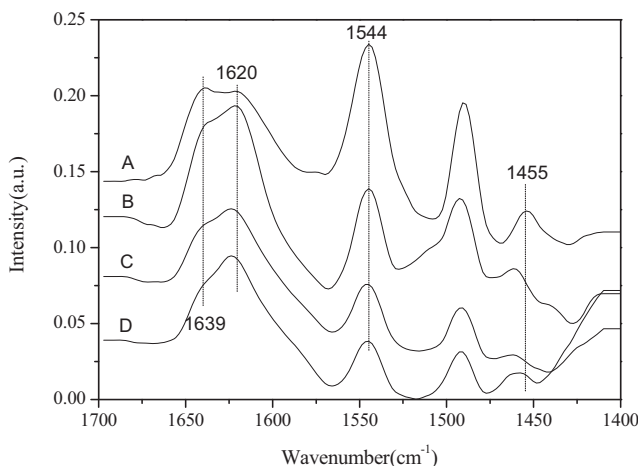


**Fig. 8.** Pyridine IR spectra of HZSM-5 and  $\text{B}_2\text{O}_3/\text{HZSM-5(E)}$  catalysts. (A) HZSM-5; (B) 3%  $\text{B}_2\text{O}_3/\text{HZSM-5(E)}$ ; (C) 9%  $\text{B}_2\text{O}_3/\text{HZSM-5(E)}$ ; (D) 15%  $\text{B}_2\text{O}_3/\text{HZSM-5(E)}$ .

adsorbed on HZSM-5 and the  $\text{B}_2\text{O}_3/\text{HZSM-5(E)}$  catalysts resulted in the appearance of bands characteristic of pyridine adsorbed on Brønsted acid sites around 1544 and 1639  $\text{cm}^{-1}$ , on Lewis acid sites at 1455 and 1622  $\text{cm}^{-1}$  [33]. It was found that the intensities of the peaks belonging to Brønsted acid sites and Lewis acid sites both decreased progressively with increasing the amount of  $\text{B}_2\text{O}_3$ . Similar to the results of  $\text{NH}_3$ -TPD characterization, the amount of Brønsted acid sites and Lewis acid sites over 15%  $\text{B}_2\text{O}_3/\text{HZSM-5(M)}$  and 15%  $\text{B}_2\text{O}_3/\text{HZSM-5(H)}$  is obviously lower than those over 15%  $\text{B}_2\text{O}_3/\text{HZSM-5(E)}$ .

Synthesis of *p*-DEB by ethylation of EB had been mostly concerned as a typical acid-catalyzed process [2]. Strong surface acidity of HZSM-5 zeolite is in favor of EB conversion but not favorable for selectivity to *p*-DEB. It was reported that the *p*-isomer was formed selectively inside the HZSM-5 channels at first, while the isomerization of the *p*-isomer proceeded just on the external surfaces and that the improvement in the *para*-selectivity by the modification was due to the inactivation of the acid sites on the external surfaces [34–36]. For this reason, it is necessary to cover the acid sites on the external surfaces of HZSM-5 zeolite to obtain the desirable selectivity for *p*-DEB. Traditionally, the technologies for passivate the acid sites on the external surfaces of zeolite by loadings of metal or non-metal oxide always caused some undesirable side-effects, such as the cover of the acid sites in the micropores of

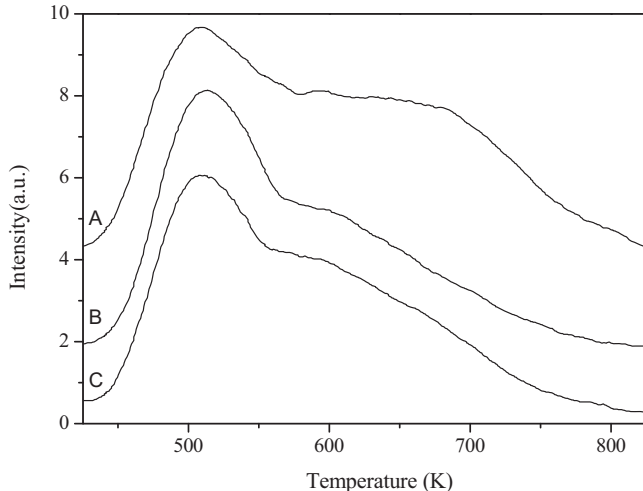


**Fig. 7.**  $\text{NH}_3$ -TPD profiles of 15%  $\text{B}_2\text{O}_3/\text{HZSM-5}$  catalysts with different precursor of  $\text{B}_2\text{O}_3$ . (A) 15%  $\text{B}_2\text{O}_3/\text{HZSM-5(E)}$ ; (B) 15%  $\text{B}_2\text{O}_3/\text{HZSM-5(M)}$ ; (C) 15%  $\text{B}_2\text{O}_3/\text{HZSM-5(H)}$ .

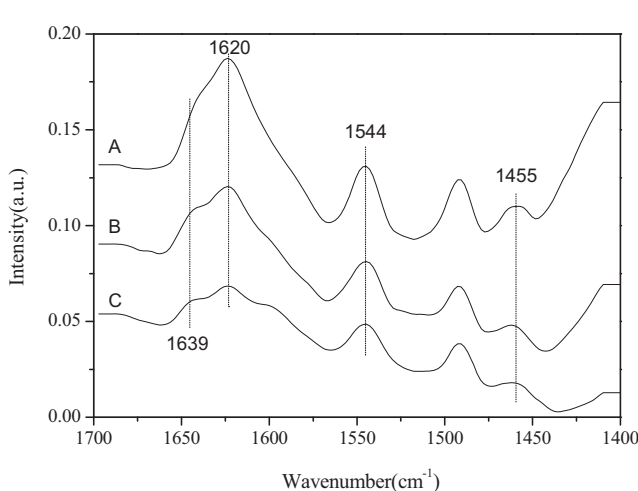
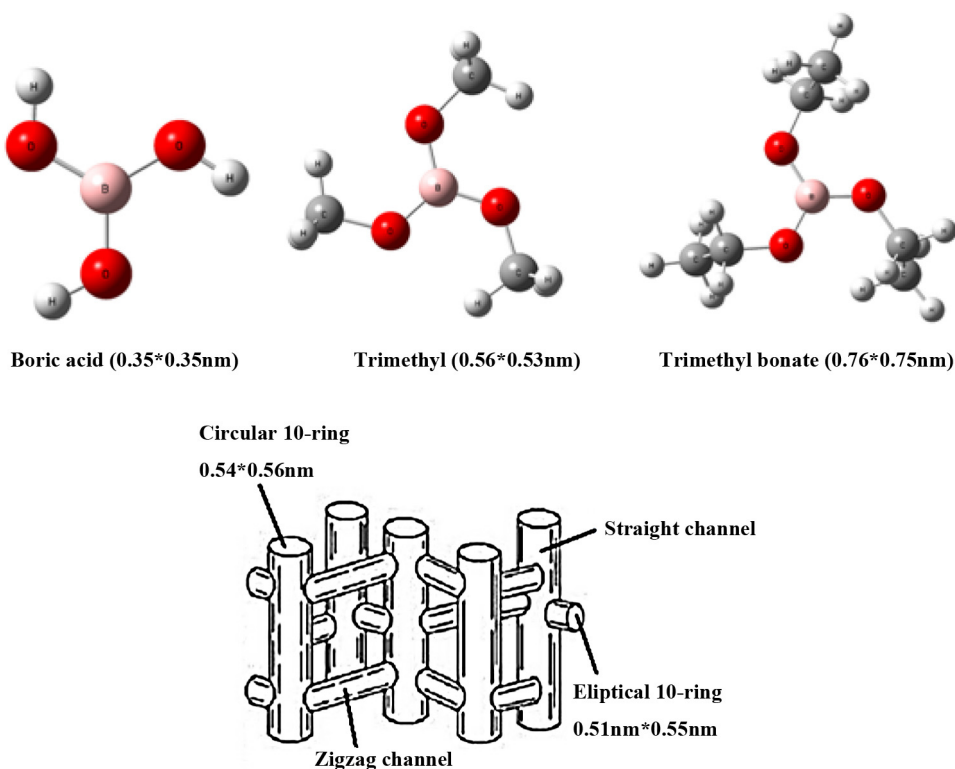


**Fig. 9.** Pyridine IR spectra of 15%  $\text{B}_2\text{O}_3/\text{HZSM-5}$  catalysts with different precursor of  $\text{B}_2\text{O}_3$ . (A) 15%  $\text{B}_2\text{O}_3/\text{HZSM-5(E)}$ ; (B) 15%  $\text{B}_2\text{O}_3/\text{HZSM-5(M)}$ ; (C) 15%  $\text{B}_2\text{O}_3/\text{HZSM-5(H)}$ .



**Scheme 1.** The molecular size of borate and the structure of ZSM-5. The molecular size of borates was obtained by ab initio method with Gaussian.

zeolite and the blockage of the partial pores of zeolite. This certainly resulted in the serious damage on the catalytic activity of zeolites. In the present study, triethyl borate was used as the precursor of  $B_2O_3$  to prepare  $B_2O_3/HZSM-5$  shape-selective catalysts. During impregnation process, triethyl borate was limited to the external surface of HZSM-5 zeolite because the molecular size of triethyl borate ( $0.76 \times 0.75$  nm) was obvious larger than the pore size of HZSM-5 zeolite ( $0.54 \times 0.56$  nm,  $0.51 \times 0.55$  nm), as shown in Scheme 1. After calcinations, the generated  $B_2O_3$  was only presented on the external surface of HZSM-5 zeolite. Meanwhile, the loadings of  $B_2O_3$  by using triethyl borate as the precursor rarely affected the acid sites in the micropores of HZSM-5 zeolite. The speculation mentioned above could be supported by the results of characterizations. As shown in Table 4, the micropore volume of 15%  $B_2O_3/HZSM-5(E)$  catalyst was  $0.117 \text{ cm}^3 \text{ g}^{-1}$ , which was slightly lower than that of parent HZSM-5 zeolite. This indicated that most of the micropores in HZSM-5 zeolite were well maintained after boron oxide modification by using triethyl borate as the precursor of  $B_2O_3$ . As shown in Fig. 6, the strong acid sites in  $B_2O_3/HZSM-5(E)$  catalysts lost obviously as characterized by NH<sub>3</sub>-TPD. Therefore, the reduction of acidity could be responsible for the improvement of the *para*-selectivity because the isomerization of *p*-DEB was suppressed due to the absence of strong acid sites. Meanwhile, the high catalytic activity was ascribed to the acid sites in the channels of HZSM-5 zeolite preserved after triethyl borate modification.

As for  $B_2O_3/HZSM-5(M)$  catalysts, although the improvement in *para*-selectivity was achieved with increasing the amount of  $B_2O_3$ , the decrease in catalytic activity was also significant. As shown in Scheme 1, the molecular size of trimethyl borate ( $0.56 \times 0.53$  nm) is similar to the pore size of HZSM-5 zeolite. Inevitably, partial trimethyl borate could enter into the pores of HZSM-5 because of its slim figure during the impregnation process. This must result in the decrease in the amount of the acid sites in the micropores of HZSM-5 zeolite and the blockage of the partial pores of

HZSM-5 zeolite. As shown in Table 5, the micropore volume of 15%  $B_2O_3/HZSM-5(M)$  catalyst was only  $0.089 \text{ cm}^3 \text{ g}^{-1}$ , which was obviously lower than that of parent HZSM-5 zeolite. This indicated that partial micropores of HZSM-5 zeolite were blocked after boron oxide modification by using trimethyl borate as the precursor of  $B_2O_3$ . Furthermore, the results of XRD and NH<sub>3</sub>-TPD were also supported the speculation mentioned above (see Figs. 1 and 7). As a result, the decrease in catalytic activity is reasonable over  $B_2O_3/HZSM-5(M)$  compared with  $B_2O_3/HZSM-5(E)$  with similar loadings of  $B_2O_3$ .

As shown in Scheme 1, the molecular size of boric acid ( $0.35 \times 0.35$  nm) was significantly lower than the pore size of HZSM-5 zeolite. Consequently, most of the boric acid was more likely to disperse in the pores of HZSM-5 zeolite during the impregnation process, and then the generated  $B_2O_3$  blocked most of the pores of HZSM-5 zeolite. As shown in Table 5, the micropore volume of 15%  $B_2O_3/HZSM-5(H)$  catalyst was only  $0.058 \text{ cm}^3 \text{ g}^{-1}$ . This contributed to the severe decrease in conversion of EB over 15%  $B_2O_3/HZSM-5(H)$  catalysts.

The activities for cracking of 1,3,5-TIPB and IPB (Table 6) were used to elucidate the acidic properties of  $B_2O_3/HZSM-5$  catalysts [37]. Compared with HZSM-5 zeolite, the conversion of 1,3,5-TIPB and conversion of IPB all decreased over all the  $B_2O_3/HZSM-5$  catalysts, which corresponded to the decrease in the amount of acid sites after loadings of  $B_2O_3$ . Among the 15%  $B_2O_3/HZSM-5$

**Table 6**  
Cracking of 1,3,5-TIPB and IPB over 15%  $B_2O_3/HZSM-5$  catalysts.

Catalysts	Conversion of 1,3,5-TIPB (%)	Conversion of IPB (%)
HZSM-5	23.8	22.4
15% $B_2O_3/HZSM-5(E)$	3.6	17.6
15% $B_2O_3/HZSM-5(M)$	5.4	13.0
15% $B_2O_3/HZSM-5(H)$	5.9	10.4

Conditions: temperature = 723 K; WHSV = 1.0 h<sup>-1</sup>.

**Table 7**

Comparison of DEC and ethanol in alkylation of EB with DEC over 15%  $B_2O_3/HZSM-5(E)$  catalysts.

Alkylation agents	Conversion of EB (%)	Products distribution of DEB (%)		
		p-DEB	m-DEB	o-DEB
DEC	31.0	97.0	2.8	0.2
Ethanol	13.4	95.2	3.5	1.3

Reaction conditions:  $T=633\text{ K}$ , 6 h,  $n(\text{EB})/n(\text{DEC or ethanol})=2:1$ , LHSV = 1  $\text{h}^{-1}$ .

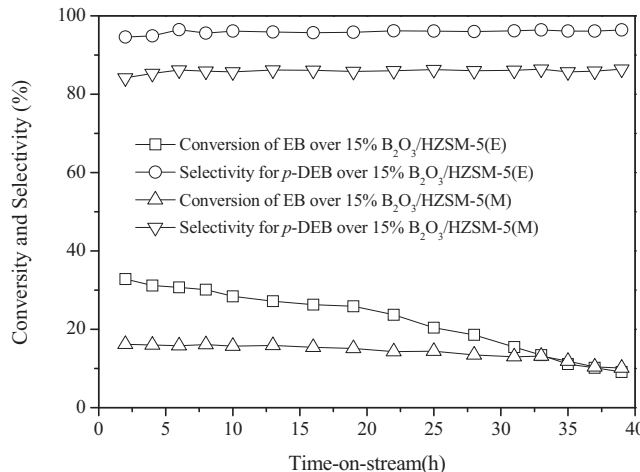


**Fig. 10.** Effects of time-on-stream on alkylation of EB with DEC over 15%  $B_2O_3/HZSM-5$  catalysts. Reaction conditions:  $T=633\text{ K}$ ,  $n(\text{EB})/n(\text{DEC})=2:1$ , LHSV = 1  $\text{h}^{-1}$ .

catalysts, the lowest conversion of 1,3,5-TIPB and the highest conversion of IPB were observed over 15%  $B_2O_3/HZSM-5(E)$  catalyst. This indicated that the cover of the acid sites on the external surface of HZSM-5 zeolite and the preservation of the acid sites in the pores of HZSM-5 zeolite were effectively achieved by loading of  $B_2O_3$  by using triethyl borate as the precursor. Consequently, the extraordinary selectivity for *p*-DEB and the higher conversion of EB were acquired over 15%  $B_2O_3/HZSM-5(E)$  catalyst.

### 3.3. Catalytic stability

**Fig. 10** shows the effects of time-on-stream on alkylation of EB with DEC over 15%  $B_2O_3/HZSM-5(E)$  catalyst and 15%  $B_2O_3/HZSM-5(M)$  catalyst. As for 15%  $B_2O_3/HZSM-5(E)$  catalyst, conversion of EB was maintained above 20% for 19 h, and then decreased gradually with time-on-stream. Only a 9.1% conversion of EB was obtained after 39 h test. By contrast with 15%  $B_2O_3/HZSM-5(E)$  catalyst, 15%  $B_2O_3/HZSM-5(M)$  catalyst exhibited a superior stability in alkylation of EB with DEC. Furthermore, the selectivity for *p*-DEB was maintained during 39 h on stream over the two catalysts, suggesting that the effect of time-on-stream on selectivity for *p*-DEB was slight.

### 3.4. Comparison of DEC with ethanol in alkylation of EB

As reported previously, DEC is a versatile compound that represents an attractive alternative to both ethyl halides and phosgene [38]. We have investigated the synthesis of EB by alkylation of benzene with DEC over ZSM-5 zeolite [39]. It was found that the activity of DEC as an alkylating agent was obviously higher than that of ethanol. In this study, the activity of DEC and ethanol in the synthesis of *p*-DEB by alkylation of EB were also investigated over 15%  $B_2O_3/HZSM-5(E)$  catalyst and the results were presented in **Table 7**. As shown in **Table 7**, conversion of EB in alkylation of EB with DEC was much higher than that in alkylation

of EB with ethanol at the same conditions. This can be ascribed to the sufficient ethyl cations during the alkylation of EB with DEC compared with ethanol. Moreover, no obvious difference in selectivity for *p*-DEB was observed in alkylation of EB with DEC or ethanol.

## 4. Conclusions

15%  $B_2O_3/HZSM-5$  catalyst prepared by using triethyl borate as a precursor for  $B_2O_3$  is highly efficient and convenient for the synthesis of *p*-DEB by alkylation of EB with DEC. During the impregnation process, triethyl borate was limited on the external surface of HZSM-5 zeolite because of its large molecular size. As a result, the generated  $B_2O_3$  is only presented on the external surface of HZSM-5 zeolite. Meanwhile, the loadings of  $B_2O_3$  by using triethyl borate as the precursor rarely affected the acid sites in the micropores of HZSM-5 zeolite. This contributed to the higher conversion of EB and the excellent shape-selectivity.  $B_2O_3/HZSM-5$  catalyst prepared by using trimethyl borate and boric acid as the precursor of  $B_2O_3$  also showed good *para*-selectivity in alkylation of EB with DEC, whereas the catalytic activity also decreased significantly. The dispersion of trimethyl borate or boric acid in the pores of HZSM-5 zeolite resulted in the decrease in the amount of the acid sites in the micropores of zeolite and the blockage of the partial pores of HZSM-5 zeolite.

## Acknowledgements

The authors thank the generous financial support from the National Natural Science Foundation of China (21076027), the Natural Science Foundation of Jiangsu College (12KJB530002), and Jiangsu Province Key Laboratory of Fine Petrochemical Engineering (KF1104).

## References

- [1] T.C. Tsai, S.B. Liu, I. Wang, *Appl. Catal. A: Gen.* 181 (1999) 355–398.
- [2] P. Wu, T. Komatsu, T. Yashima, *Microporous Mesoporous Mater.* 22 (1998) 343–356.
- [3] K.U. Nandhini, B. Arabindoo, M. Palanichamy, V. Murugesan, *Catal. Commun.* 7 (2006) 351–356.
- [4] K.U. Nandhini, B. Arabindoo, M. Palanichamy, V. Murugesan, *Microporous Mesoporous Mater.* 81 (2005) 59–71.
- [5] S.M. Waziri, S. Al-Khattaf, *Ind. Eng. Chem. Res.* 48 (2009) 8341–8348.
- [6] I. Wang, C.L. Aye, B.J. Lee, M.H. Chen, *Proceedings of the Ninth International Congress on Catalysis*, Calgary, 1988.
- [7] X.X. Guan, N. Li, G.J. Wu, J.X. Chen, F.X. Zhang, N.J. Guan, *J. Mol. Catal. A: Chem.* 248 (2006) 220–225.
- [8] T. Hibino, M. Niwa, Y. Murakami, *J. Catal.* 128 (1991) 551–558.
- [9] J.H. Kim, A. Ishida, M. Okajima, M. Niwa, *J. Catal.* 161 (1996) 387–392.
- [10] J. Das, Y.S. Bhat, A.B. Halgeri, *Catal. Lett.* 20 (1993) 349–357.
- [11] R.W. Weber, K.P. Moller, C.T. O’Conner, *Microporous Mesoporous Mater.* 35 (2000) 533–543.
- [12] Z.R. Zhu, Q.L. Chen, Z.K. Xie, W.M. Yang, D.J. Kong, C. Li, *J. Mol. Catal. A: Chem.* 248 (2006) 152–158.
- [13] F. Bauer, W.H. Chen, Q. Zhao, A. Freyer, S.B. Liu, *Microporous Mesoporous Mater.* 47 (2001) 67–77.
- [14] F. Bauer, W.H. Chen, E. Bilz, A. Freyer, V. Sauerland, S.B. Liu, *J. Catal.* 251 (2007) 258–270.
- [15] Y.G. Li, W.H. Xie, S. Yong, *Appl. Catal. A: Gen.* 150 (1997) 231–242.
- [16] A. Martinsa, J.M. Silva, C. Henriques, F.R. Ribeiro, M.F. Ribeiro, *Catal. Today* 107–108 (2005) 663–670.

- [17] P. Kovacheva, A. Predoeva, K. Arishtirova, S. Vassilev, *Appl. Catal. A: Gen.* 223 (2002) 121–128.
- [18] V.N. Sheemol, B. Tyagi, R.V. Jasra, *J. Mol. Catal. A: Chem.* 215 (2004) 201–208.
- [19] B. Xue, Y.X. Li, L.J. Deng, *Catal. Commun.* 10 (2009) 1609–1614.
- [20] B. Xue, H. Li, J. Xu, P. Liu, Y. Zhang, Y. Li, *Catal. Commun.* 29 (2012) 153–157.
- [21] L. Fu, B. Xue, J. Xu, W. Zhang, Y. Li, *Speciality Petrochem. (China)* 29 (2012) 48–53.
- [22] Y. Zhang, B. Xue, J. Xu, P. Liu, Y. Li, *Petrochem. Technol. (China)* 41 (2012) 277–282.
- [23] J. Zhang, B. Xue, J. Xu, P. Liu, Y. Li, *J. Mol. Catal. (China)* 25 (2011) 514–519.
- [24] B. Xue, J. Su, Q. Huang, J. Xue, Y.X. Li, *Catal. Commun.* 45 (2014) 49–53.
- [25] S.B. Kulkarni, V.P. Shiralkar, A.N. Kotasthane, R.B. Borade, P. Ratnasamy, *Zeolites* 2 (1982) 313–318.
- [26] E. Mei, A.M. Bardo, M.M. Collinson, D.A. Higgins, *J. Phys. Chem. B* 104 (2000) 9973–9980.
- [27] J.C. Jansen, F.J. van der Gaag, H. van Bekkum, *Zeolites* 4 (1984) 369–372.
- [28] Y. Zhang, M.Q. Wang, *Mater. Sci. Eng. B* 49 (1997) 205–210.
- [29] Y. Zhang, M.Q. Wang, D. Wu, *Mater. Lett.* 35 (1998) 144–150.
- [30] L. Gora, B. Sulikowski, E.M. Serwicka, *Appl. Catal. A: Gen.* 325 (2007) 316–321.
- [31] C. Hidago, H. Itoh, T. Hattori, M. Niwa, Y. Murakami, *J. Catal.* 85 (1984) 362–369.
- [32] F. Lonyi, J. Valyon, *Microporous Mesoporous Mater.* 47 (2001) 293–301.
- [33] V.V. Ordovsky, I.I. Ivanova, E.E. Knyazeva, V.V. Yuschenko, V.I. Zaikovskii, *J. Catal.* 295 (2012) 207–216.
- [34] G. Paparatto, E. Moretti, G. Leo, F. Gatti, *J. Catal.* 105 (1987) 227–232.
- [35] T. Yashima, Y. Sakaguchi, S. Namba, *Stud. Surf. Sci. Catal.* 7 (1981) 739–751.
- [36] J.H. Kim, S. Namba, T. Yashima, *Zeolites* 11 (1991) 59–63.
- [37] Y. Sugi, Y. Kubota, K. Komura, N. Sugiyama, M. Hayashi, J.H. Kim, G. Seo, *Appl. Catal. A: Gen.* 299 (2006) 157–166.
- [38] Z. Zhang, X.B. Ma, P.B. Zhang, Y.M. Li, S.P. Wang, *J. Mol. Catal. A: Chem.* 266 (2007) 202–206.
- [39] Y.X. Li, B. Xue, X.Y. He, *J. Mol. Catal. A: Chem.* 301 (2009) 106–113.